

Source mechanism of the 1998 M_w 7.4 intraplate strike-slip earthquake in the West Philippine Basin revealed by Coulomb stress changes



Yi-Chin Lin, Jing-Yi Lin *

Department of Earth Sciences, National Central University, 300 Jhongda Road, Jhongli City, Taoyuan County 32001, Taiwan

ARTICLE INFO

Article history:

Received 27 February 2015
 Received in revised form 5 October 2015
 Accepted 29 November 2015
 Available online 23 December 2015

Keywords:

Static Coulomb Failure Stress
 Subduction
 Oceanic plate
 Strike-slip earthquake
 Seismicity rate

ABSTRACT

On April 11, 2012, M_w 8.6 and M_w 8.2 earthquakes occurred off the west coast of northern Sumatra as a result of strike-slip type events within the Indo-Australia plate. It is suggested that these two earthquakes were linked to the occurrence of the 2004 great Sumatra–Andaman earthquake. Over the last few decades, several strike-slip type earthquakes have been observed within the West Philippine Basin (WPB). However, little investigation has been conducted to understand these strike-slip earthquakes and the possible geohazard potential that they may bring. In our study, to determine the rupture plane for these strike-slip events, we calculated the static Coulomb Failure Stress changes (Δ CFS) induced by the 1998 M_w 7.4 strike-slip earthquake and compared them with the distribution of aftershocks. Our results show that when the fault plane is trending in the NW–SE direction, the aftershocks that occurred in the region show a good agreement with the maximal positive Δ CFS. Consequently, instead of sliding along the pre-existing oceanic fracture zones, the 1998 strike-slip event that occurred in the WPB should have ruptured in the NW–SE direction. Moreover, we also observed a correlation between the activities of the normal faulting type earthquakes along the trench and the positive Δ CFS induced by the 1998 M_w 7.4 event, which suggests that the occurrence of intraplate strike-slip events in oceanic plates might affect the distribution of earthquakes along the nearby subduction systems.

© 2015 Elsevier B.V. All rights reserved.

1. Introduction

Generally, earthquakes that occur around subduction systems involve a thrust faulting mechanism due to the plate convergence or normal faulting origins because of the plate bending or the back-arc opening effect. However, the great M_w 8.6 and M_w 8.2 earthquakes that occurred in the southwestern offshore of the Sumatra Trench on April 11, 2012 (inset in Fig. 1), were strike-slip earthquakes, which created interest in the origin of such unusual events and the possible geohazard potential that they may bring. Historically, most of the events in the region have been interpreted as the activity of the NNE–SSW trending oceanic fracture zones (brown lines in inset of Fig. 1) (Deplus et al., 1998; Lin et al., 2009). However, based on several seismic methods, a more complex explanation for the rupture dynamics was proposed (Meng et al., 2012; Yue et al., 2012).

East of Taiwan, the Philippine Sea Plate (PSP) is subducting northwestward beneath the Eurasian Plate (EU) along the Ryukyu Trench (RT) at a convergence rate of 8–9 cm/year (Yu et al., 1997) (Fig. 1). South of RT, the oceanic basin is characterized by several NE–SW trending oceanic fractures, as evidenced by the bathymetry (Chang, 2007), and free-air gravity anomalies (Hsu et al., 2013). A majority of the earthquakes have occurred around the subduction

system and are characterized by a thrust faulting mechanism along the plate interface and by normal faulting in the back-arc, fore-arc basin and outer-rise area. However, some intraplate strike-slip earthquakes have been observed in the West Philippines Basin (WPB) in the vicinity of the oceanic fracture zones (Fig. 1). On May 3, 1998, a M_w 7.4 strike-slip earthquake occurred within the WSP, to the south of RT and to the east of Gagua Ridge (GR) (Fig. 1). The hypocenter coincided with the Luzon–Okinawa Fracture Zones (LOFZ), showing a significant resemblance in the tectonic context with the west coast of northern Sumatra. It is thus intriguing to know whether the earthquakes that occurred in the western offshore of Sumatra and WPB possess similar seismogenic conditions and rupture characteristics. However, no clear identification of the rupture plane has been determined.

In addition, following the event of May 3, 1998, several strike-slip earthquakes of similar focal mechanism, with one fault plane sub-parallel to approximately $N35^\circ E$, also occurred in the WPB (Fig. 1) (Lin et al., 2013a, 2013b). Among them, an earthquake sequence started with the M_w 6.7 event of August 17, 2009, which occurred approximately 200 km from the 1998 mainshock area (Fig. 1). Several previous studies have already illustrated that a large earthquake could transfer stress over a wide distance. The static Coulomb Failure Stress changes (Δ CFS) are widely used to investigate the impact of large earthquakes on aftershock distribution and seismicity rate changes (Harris, 1998; Lin and Stein, 2004; Ma et al., 2005; Nostro et al., 2005; Parsons et al.,

* Corresponding author. Tel.: +886 34227151x65613; fax: +886 34222044.
 E-mail address: jylin.gep@gmail.com (J.-Y. Lin).

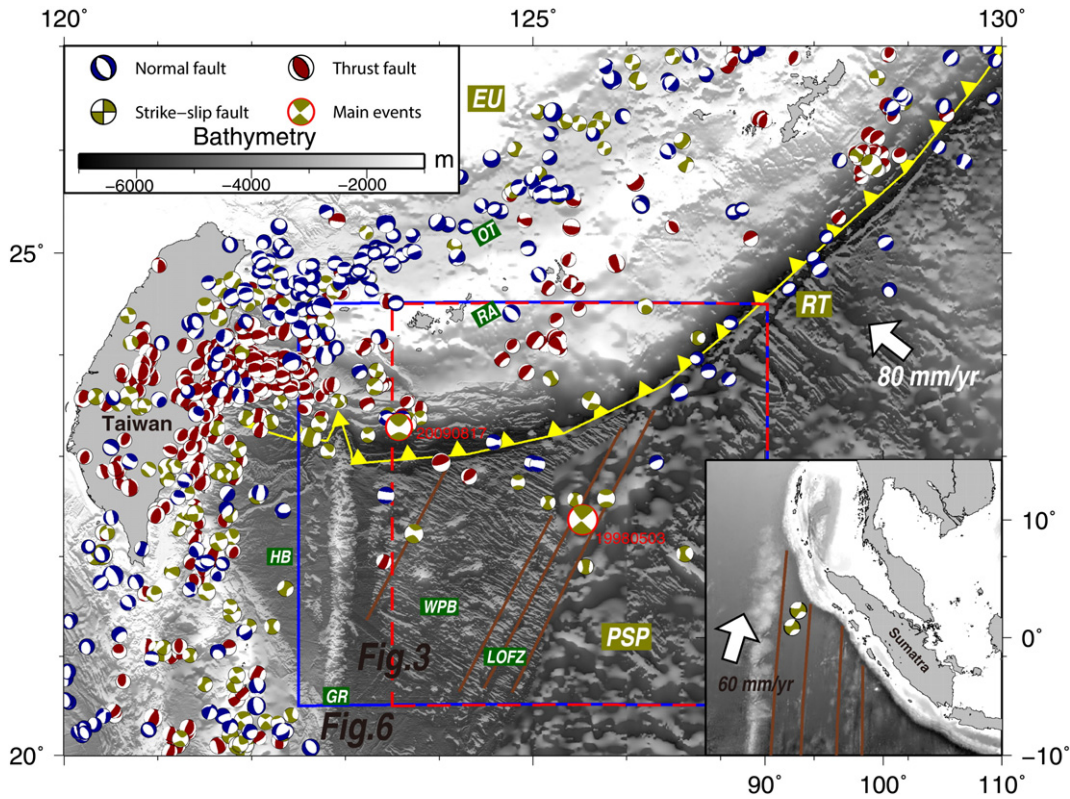


Fig. 1. Map view of the main tectonic features and focal mechanisms for the East Taiwan and Western Philippine Basin (WPB) area. The plate motion of the West Philippine Plate toward the Eurasian Plate is approximately 80–90 mm/year in the direction of N 306°–312° (Yu et al., 1997), which is shown by the white arrow. The focal mechanisms are extracted from the Globe Central Moment Tensor (GCMT) catalog (<http://www.globalcmt.org/>) (Dziewonski et al., 1981) for the time period from January 1, 1976, to August 31, 2014. The depth range is between 10 and 306 km. The focal mechanism with red contour is the position of the M_w 7.4 earthquake of May 3, 1998. The brown, blue and dark green focal mechanisms show compressive, extensional and strike-slip events, respectively. The brown lines represent the position of the oceanic fracture zone (Chang, 2007; Hsu et al., 2013). The red dashed rectangle shows the area of Figs. 3 and 5; the blue rectangle shows the area of Fig. 6. PSP: Philippine Sea Plate; EU: Eurasia Plate; HB: Huatung Basin; LOFZ: Luzon–Okinawa Fracture Zones; GR: Gagua Ridge; RA: Ryukyu Arc; OT: Okinawa Trough.

1999; Wang and Chen, 2001). An increase of certain amount of stress change is adequate to trigger events and affect the location of aftershock sequences. (Arnadóttir et al., 2003; Harris, 1998). Based on this assumption, there should be a strong probability that the strike-slip earthquakes occurred in the WPB after the 1998 M_w 7.4 earthquake could be the result of such a stress triggering process caused by the 1998 mainshock.

Around and in the WPB area, the seismogenic and tsunamigenic properties of the Ryukyu subduction system have been largely investigated (Ando et al., 2009; Hsu et al., 2013; Lin et al., 2014; Nakamura, 2006, 2009). However, little investigation has been performed in the oceanic domain within the WPB. In view of the 2012 M_w 8.2 and M_w 8.6 earthquakes in the offshore west coast of northern Sumatra, a greater understanding regarding the oceanic intraplate earthquakes is indispensable. In our study, we calculated the Δ CFS induced by the 1998 M_w 7.4 strike-slip earthquake and we compared the aftershock distribution with the estimated Δ CFS to obtain better constraints for the orientation of the fault surface.

2. Method and data processing

2.1. Static coulomb stress changes (Δ CFS)

The Δ CFS is defined as

$$\Delta\text{CFS} = \Delta\tau + \mu(\Delta\sigma + \Delta P) \quad (1)$$

where $\Delta\tau$ is the shear stress change along the slip direction on a given failure plane, μ represents the effective friction coefficient, $\Delta\sigma$ is the change in effective normal stress (positive for extension) and ΔP is the

pore pressure changes (Harris, 1998). The pore pressure changes ΔP is usual proportional to the volumetric stress changes under undrained condition, as shown by the Eq. (2).

$$\Delta P = -B \frac{\Delta\sigma_{kk}}{3} \quad (2)$$

where B is the Skempton coefficient (Skempton, 1954) with a range between 0.5 and 1 depend on the rock material. $\Delta\sigma_{kk}$ is the value of normal stress. In the isotropic case, $\Delta\sigma_{11} = \Delta\sigma_{22} = \Delta\sigma_{33}$ and $\Delta\sigma_{kk}/3 = \Delta\sigma$ (average stress) (see Cocco and Rice, 2002), thus

$$\Delta P = -B\Delta\sigma. \quad (3)$$

By substituting Eq. (3) in Eq. (1), we can get the following equation:

$$\Delta\text{CFS} = \Delta\tau + \mu'\Delta\sigma \quad (4)$$

where $\mu' = \mu(1 - B)$. Generally, the parameter μ' varies within the range of 0.0–0.8, depending on the magnitude of the cumulative slip or the pore fluid pressure (King et al., 1994; Stein et al., 1992). When the pore pressure becomes higher, the value of μ' is smaller. However, because information was scarce regarding the rock properties around our study area, we assumed an average value of 0.4 for μ' . A homogeneous and isotropic half-space elastic medium was also assumed (Okada, 1985). In our study, Coulomb 3.3 software from USGS (<http://earthquake.usgs.gov/research/software/coulomb/>) was used for the calculation. During the estimation, two types of receiver faults can be created: the specific and optimally oriented receiver faults. The former assumes that both the source and receiver faults have the same fault parameters, whereas the latter accounts

for the stress perturbation caused by the mainshock for a specific fault parameter. To determine the rupture parameters for the source fault, we applied the empirical relations shown as below:

$$M_w = 4.33 + 1.49 * \log(\text{RLD}) \quad (5)$$

$$M_w = 3.80 + 2.59 * \log(\text{RW}) \quad (6)$$

$$M_w = 7.04 + 0.89 * \log(\text{AD}) \quad (7)$$

where M_w is the moment magnitude, RLD is the subsurface rupture length (km), RW represents the downdip rupture width (km), and AD shows the average displacement (m) (Wells and Coppersmith, 1994). Furthermore, the uniform slip model with linear tapering is used for the estimation of the fault slip distribution.

2.2. Data processing

One main objective of our study was to find the fault plane along which the ΔCFS generated by the mainshock corresponded to the aftershock distribution. Thus, we first used the focal mechanisms of the Global Centroid Moment Tensor (GCMT) catalog (Dziewonski et al., 1981) to determine the fault planes solution, and the ΔCFS was initially calculated based on the geometries of the two fault planes of the mainshock focal mechanism. To avoid the possible uncertainty of the focal mechanism, we also determined a fault plane solution by tracing how the aftershocks occurred within one month after the occurrence of the mainshock. In addition, we noticed that several focal mechanisms with the compressive and extensional mechanism occurred north of the mainshock (Fig. 1). To consider the possible effects caused by such a complex regional stress field, we simulated the ΔCFS associated with the 1998 mainshock by using the extensive and compressive focal

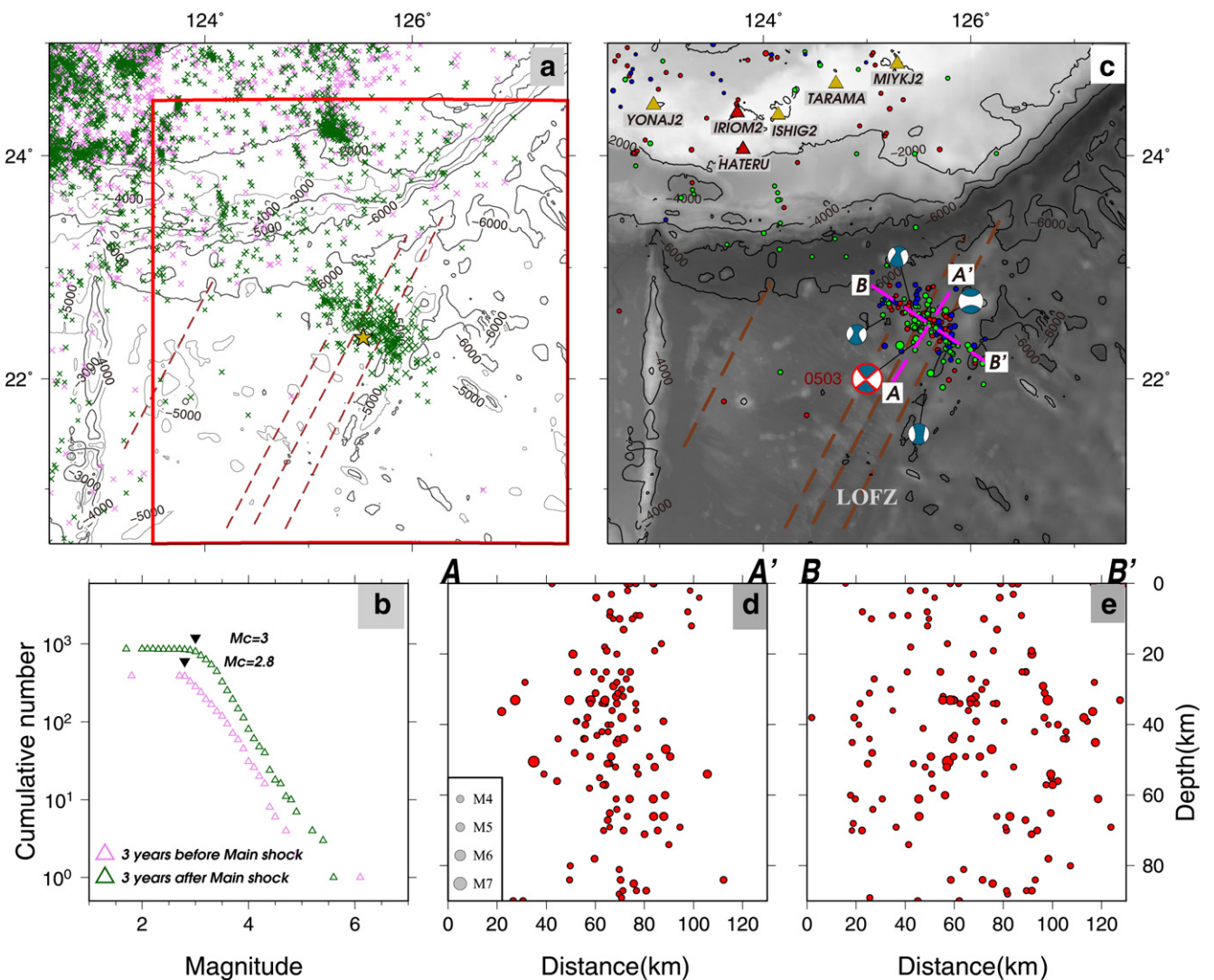


Fig. 2. Aftershock distribution and the estimation of the magnitude of completeness M_c . (a) Earthquakes occurred 3 years before and after the 1998 M_w 7.4 earthquake are extracted from the reviewed International Seismological Center (ISC) catalog (<http://www.isc.ac.uk/iscbulletin/search/catalogue/>) and represented by the pink and green crosses, respectively. The depth range of these selected earthquakes is between 0 and 124 km. The red rectangle shows that area of Figs. 3 and 5. (b) The relation of the cumulative number and magnitude of the earthquakes shown by pink and green crosses in (a) and the magnitude of completeness M_c is estimated at 2.8 and 3.0, respectively. The aftershocks with $M_w \geq 3.0$ that occurred within one month after the mainshock are shown in (c). The red, green and blue dots show the earthquake depths of 0–30 km, 30–60 km and larger than 60 km, respectively. The blue color focal mechanisms represent the sequence of the May 3, 1998, M_w 7.4 earthquake. The focal mechanisms with the red contour are the position of the mainshock. The brown dashed lines show the LOFZ. The red and yellow triangles are the seismic stations for the Japan Meteorological Agency (JMA) network. The two purple dashed lines are the position of the two cross sections AA' and BB'. AA' is sub-parallel to the LOFZ, whereas BB' trends approximately along the direction of the plate motion. The distribution of aftershocks along AA' and BB' cross-sections is represented in (d) and (e) in which the radius of circles represents the magnitude of earthquakes.

mechanisms as the optimally oriented receiver faults. Hypocenters and magnitudes extracted from the International Seismological Center (ISC) catalog (<http://www.isc.ac.uk/iscbulletin/search/catalogue/>), which contains events determined from several local networks, were used to estimate the pre-shock and aftershock seismicity (Fig. 2a). As static Δ CFS induced by a mainshock can trigger earthquakes at great distance and after a long period of time, the pre-shock and aftershock are determined not only for the earthquakes occurred along the fault rupture, but also for the events occurred at near and intermediate distances from the mainshock in our study. At the end of January 1999, two seismic stations, IRIOM2 and HATERU, were added around Ishigaki Island by the Japan Meteorological Agency (JMA) (red triangles in Fig. 2c). In addition, two other stations (YONAJ2 and YONAGU) were displaced to have a better reception for the earthquakes nearby Ryukyu Trench. To avoid the possible influence induced by the improvement of the seismic network for the earthquake statistic, we estimate and compare the magnitude of completeness (M_c) for the earthquakes obtained before and after the mainshock (Fig. 2b). M_c is the magnitude at which 90% of the earthquakes can be modeled by a power law fit (Wiemer and Wyss, 2000). The distributions of M_c show a relatively more complete record for the aftershock period. Finally, a M_c of 2.8 and 3 were obtained for the data before and after the 1998 mainshock. Generally, more advanced equipments should provide relatively more complete and precise dataset. Thus, we set the value of 3 obtained from the data recorded after the 1998 mainshock to be the minimal magnitude acquired for the selection of aftershocks to ensure the consistency in the comparison. In total, 1633 reviewed earthquakes from ISC during the period from May 3, 1995, to May 3, 2001, were used.

3. Results

3.1. Determination of fault plane parameters

The fault parameters used in this study are summarized in Table 1. The first two fault planes were determined from the GCMT catalog. As shown in Fig. 1, the first nodal plane strikes along the 139° direction (hereafter called F1), whereas the other lies along the 49° direction (hereafter called F2) (Table 1). The M_w of the mainshock was 7.4. Then, the rupture parameters were estimated to be 115 km in length, 24.54 km in width, and 1.65 m in average displacement according to the empirical law illustrated by Eqs. (5) to (7) (Wells and Coppersmith, 1994). Other two fault planes were determined from the aftershocks distribution within one month after the mainshock. Based on the plane view, the distribution of 1-month aftershocks with $M_w \geq 3.0$ demonstrated a predominant NW–SE trending feature which seemed to be a possible candidate for the fault plane (Fig. 2c). Thus, a strike of 127° was obtained for the rupture parameter (F1'), which differed, by approximately 12° from the fault plane F1 (Table 1). Taking into account the conjugate fault plane of F1', we also rotated the F2 12° counterclockwise to create another fault plane, F2'. The rupture length of F1', determined from the aftershock distribution, shows a good agreement with that of F1, which was estimated

from the magnitude by the empirical law. The aftershock distribution along the AA' profile shows that the width of F1' is approximately 20 to 30 km (Fig. 2d). However, no clear lineaments of the aftershock distribution were observed along the BB' cross-section (Fig. 2e).

3.2. Δ CFS for the specific receiver faults identical to the mainshock

The depth of the Δ CFS calculation was firstly set at the epicenter (in this case, 22.9 km). Basically, the Δ CFS calculated for the receiver faults F1, F2, F1' and F2' shows similar patterns (Fig. 3). Both the north and south areas of the fault plane are characterized by an obvious negative Δ CFS distribution. The positive Δ CFS is located at both ends of the rupture surface for all the results. However, the difference in the orientation of the maximal Δ CFS area is distinct. The maximal Δ CFS area trends primarily along the NW–SE direction for the calculations based on F1 and F1' (Fig. 3a and c), whereas the maximal Δ CFS area trends primarily along the NE–SW direction for the estimations based on F2 and F2' (Fig. 3b and d). If we compare the aftershock distribution (black crosses in Fig. 3) with the Δ CFS patterns, all of the results show that many earthquakes occurred in the negative Δ CFS area. Most of these events were located along the fault plane and farther north in the Ryukyu subduction system (gray dashed rectangle in Fig. 3a). At first glance, this result does not correspond to the general concept that the earthquakes should occur in the positive Δ CFS area. However, the earthquakes in the north of RT have thrusting-type mechanism, but the receiver fault is strike-slip type in the calculation (Figs. 1 and 3). Thus, the earthquake cluster located in the north of RT could not correspond to the positive Δ CFS area. For the earthquakes located along the mainshock fault plane where the Δ CFS is purely negative, the occurrence of aftershocks might be due to the dynamic stress transfer process, instead of static one. In consequence, the occurrence of the aftershocks along the fault plane generally possesses more complicated stress transfer procedure and could not be discussed with the presence of positive Δ CFS. Otherwise, the majority of the earthquakes that occurred in the positive Δ CFS area were located to the northwest of the fault plane. When the receiver fault is F1 or F1', the aftershocks in the positive Δ CFS area are distributed at the northwest side of the fault plane and trend along the NW–SE direction. This pattern is consistent with the orientation of the maximal Δ CFS pattern (Fig. 3a and c). However, no such correlation was observed when the fault plane is F2 or F2' (Fig. 3b and d). Even the Δ CFS to the northwestern of fault plane has positive value; the shape of the positive Δ CFS is trending NE–SW direction, which does not consistent with the aftershocks distribution. In addition, when the F2 or F2' is the receiver fault, almost no earthquakes occurred in the area where we observed the maximal Δ CFS value.

To analyze the Δ CFS variation at depths, the Δ CFS along two cross-sections A1A1' and A2A2' were evaluated when the receiver fault plane is F1' (Fig. 4a and c). Δ CFS distribution along two cross-sections B1B1' and B2B2' were evaluated when the receiver fault plane is F2' (Fig. 4b and d). The A1A1' and B1B1' profiles cut through the fault

Table 1
The focal parameters used for the estimation of Δ CFS. The unit of strike, slip, and rake is degree.

Label	Strike	Dip	Rake	Determination base on
F1	139	82	1	Nodal plane 1 of the focal mechanism for the 1998/05/03 M_w 7.4 earthquake
F1'	127	82	1	Aftershock distribution of the 1998/05/03 M_w 7.4 earthquake
F2	49	89	172	Nodal plane 2 of the focal mechanism for the 1998/05/03 M_w 7.4 earthquake
F2'	37	89	172	The rotation of F2 by the intersection angle of F1 and F1'
E1	86	46	−119	Focal mechanism for the 2001/11/25 M_w 5.5 earthquake
E2	258	45	−121	Focal mechanism for the June 2010/06/30 M_w 5.3 earthquake
T1	247	19	120	Focal mechanism for the 2001/02/08 M_w 5.8 earthquake
2009 earthquake	134	76	8	Focal mechanism for the 2009/08/17 M_w 6.7 earthquake

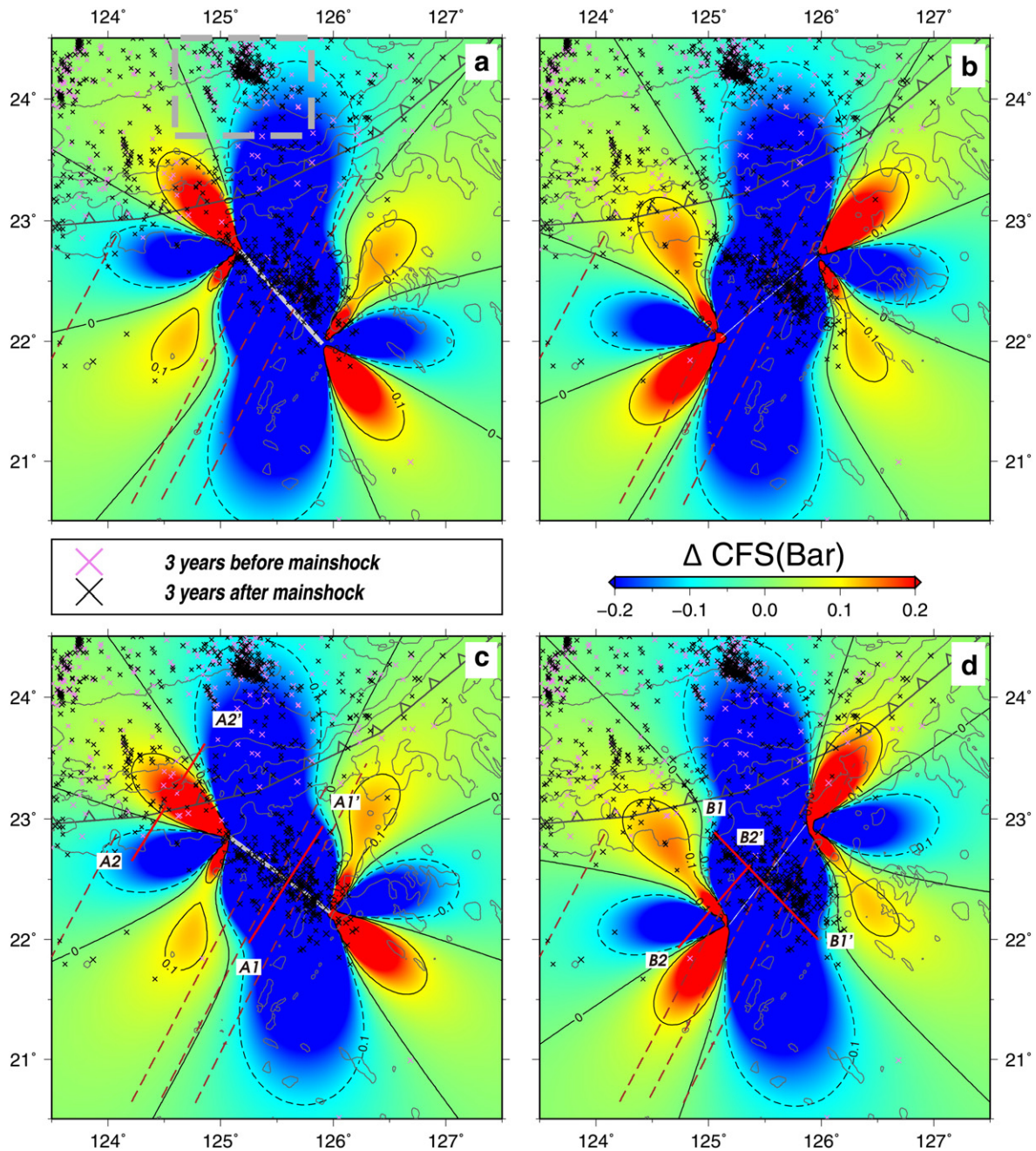


Fig. 3. The Coulomb Failure Stress changes (ΔCFS) (in Bars) induced by the May 3, 1998, M_w 7.4 mainshock at a depth of 22.9 km. The distribution of the 3-year pre-shocks and aftershocks with a magnitude $M_w \geq 3.0$ extracted from ISC catalog are shown by pink and black crosses. The white line is the slip plane projected on the surface. (a) to (d) show the results calculated when the receiver fault is F1, F2, F1', and F2', respectively. The red lines in (c) and (d) show the position of cross-sections shown in Fig. 4. The dashed brown lines are the oceanic fracture zones. The gray line with triangle represents Ryukyu Trench.

plane, whereas the A2A2' and B2B2' cross the area where we observed the most aftershocks and relatively larger ΔCFS (Fig. 3c and d). The ΔCFS of the fault intersecting cross-sections (A1A1' and B1B1') shows a dominant negative ΔCFS value at the area near the source depth. However, when the depth is slightly shallower or deeper, the ΔCFS turns to positive (Fig. 4a and b). In contrast, when the cross-sections are located outside the fault plane (A2A2' and B2B2'), the ΔCFS shows identical pattern at all depths (Fig. 4c and d). In any case, except for the earthquakes occurred along the mainshock fault plane, almost all the aftershocks are located in the area where the ΔCFS is positive. Particularly, more aftershocks occurred in the positive ΔCFS area along A2A2' than along B2B2' (Fig. 4c and d).

3.3. ΔCFS for other constructed receiver faults

Because of the variety of earthquake mechanisms occurring in the study area, the estimation of ΔCFS based only on the strike-slip fault plane may not be sufficient to explain the presence of no strike-slip events. Thus, we used three sets of fault parameters, T1, E1 and E2 (Table 1), as the receiver fault to estimate the effect induced by the 1998 mainshock on other types of earthquakes. Since the ΔCFS calculated based on F1 and F1' or F2 and F2' is similar. We only show the results estimated when the source faults are F1' and F2' (Fig. 5). T1 represents the fault plane of the thrusting-type event, which is determined from the focal mechanisms in the area and has a direction

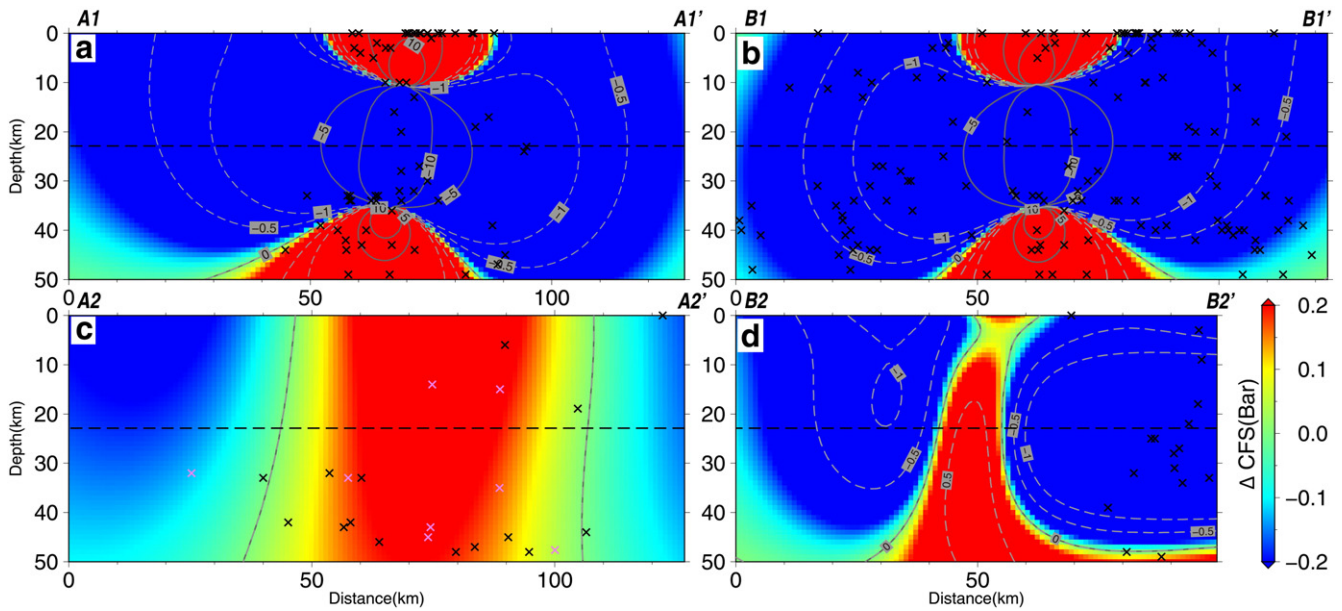


Fig. 4. The Δ CFS distribution along the cross-sections A1A1', A2A2', B1B1' and B2B2' indicated in Fig. 3c and d. The pre-shocks and aftershocks which occurred within 15 km from the profile are shown by the pink and black crosses.

sub-parallel to the trench (Fig. 5a and c). When the source fault is F1', the Δ CFS calculated for the compressive mechanism shows a dominant NNW–SSE trending distribution of positive value (Fig. 5a). This positive area is limited to the south of 23.5°N and shows a relatively small influence of large Δ CFS on the geographical scale. Only two obvious negative Δ CFS areas occurred south of the RT. The west one is relatively closer to the RT, whereas the east one is located in the WPB. In the area with positive Δ CFS, we observed a relatively larger number of events with compressive focal mechanisms (gray dashed rectangle in Fig. 5a). When the source fault is F2', the Δ CFS has similar pattern (Fig. 5c) with a N–S trending positive zone and two negative areas at the two end of the fault. However, the size of the negative area is relatively smaller.

E1 and E2 are the fault planes determined from the normal faulting events (Fig. 5b and d). The Δ CFS calculated based on E1 and E2 as specific receiver fault had a very similar pattern. Thus, we only show the calculation of Δ CFS based on E1 (Fig. 5b and d). When the source fault is F1', the Δ CFS distribution based on the extensional event shows that the negative values are widely distributed along the NS direction, crossing over the oceanic plate and dominating the area between 125°E and 126°E. To both sides of this negative Δ CFS, the Δ CFS shows positive values. Extensional events can only be observed in the areas with positive Δ CFS (Fig. 5b). In contrast, when the source fault is F2', the western positive Δ CFS area does not correspond to the position of extensional events at all (Fig. 5d).

4. Discussion

4.1. Main fault plane for the 1998 strike-slip earthquake in the WPB

We observed a good correlation between the aftershock distribution and the maximal Δ CFS area when the source and receiver fault is strike-slip type and along F1 or F1'. Thus, instead of slipping along the LOFZ which has NE–SW orientation, the 1998 mainshock appears to rupture along the NW–SE direction (F1, F1'), almost orthogonal to the LOFZ. Moreover, the Δ CFS obtained from the fault plane F1' determined from the aftershocks shows a relatively better correlation between the aftershocks and the positive Δ CFS (Fig. 3a and c). The aftershock distribution corresponds almost exactly to the area where the Δ CFS is

positive. In addition, the distribution of normal faulting earthquakes also has a good agreement with the positive Δ CFS when the source fault is F1'. Thus, the F1' fault plane appears to be the most likely fault plan for the 1998 M_w 7.4 event.

4.2. The influence of the oceanic intraplate earthquakes on the subduction-related earthquakes

For the Δ CFS distribution calculated for the extensional mechanism (Fig. 5b and d), the most obvious feature is the dominant NS trending negative Δ CFS between 125°E and 126°E. Coincidentally, though numerous extensional focal mechanisms occurred along the RT in the outer rise area, no extensional event was reported between 125°E and 126°E in the negative Δ CFS area (Fig. 1). Particularly, when the source fault is F1', we found the presence of normal faulting events in the positive Δ CFS area, located to both sides of the negative Δ CFS (Fig. 5b). This observation suggests that the Δ CFS induced by the 1998 M_w 7.4 event could affect the distribution of the outer rise seismicity in the subduction system. For the estimation of Δ CFS of the thrusting event (Fig. 5a and c), we found that the positive Δ CFS pattern corresponds well to the distribution of thrusting-type earthquakes. However, the cluster with the highest density of thrusting events was located in the area where the Δ CFS was relatively smaller (Fig. 5a and c). In addition, the seismicity rate was not increased significantly after the occurrence of the mainshock. Thus, no direct correlation between the activity of the thrusting event that occurred along the plate interface and the 1998 M_w 7.4 strike-slip event can be derived. Previous research shows that the crustal stress in the subduction system could be influenced by the subducted bathymetric features (Wu et al., 2010). Our study area is located at the intersection between the LOFZ and the Ryukyu subduction system. Thus, the insignificant relationship between the thrusting events and the Δ CFS of the 1998 mainshock may be caused by the change of stress environment when the plate subducts. On the contrary, the extensional events are located in the outer rise area, which are still in the oceanward side of the trench, and the influence of the Δ CFS induced by the oceanic intraplate event could persist. Consequently, we suggest the 1998 M_w 7.4 event did enhance the occurrence of earthquakes in the subduction system. However, this influence seems to be disturbed when the oceanic plate starts to subduct.

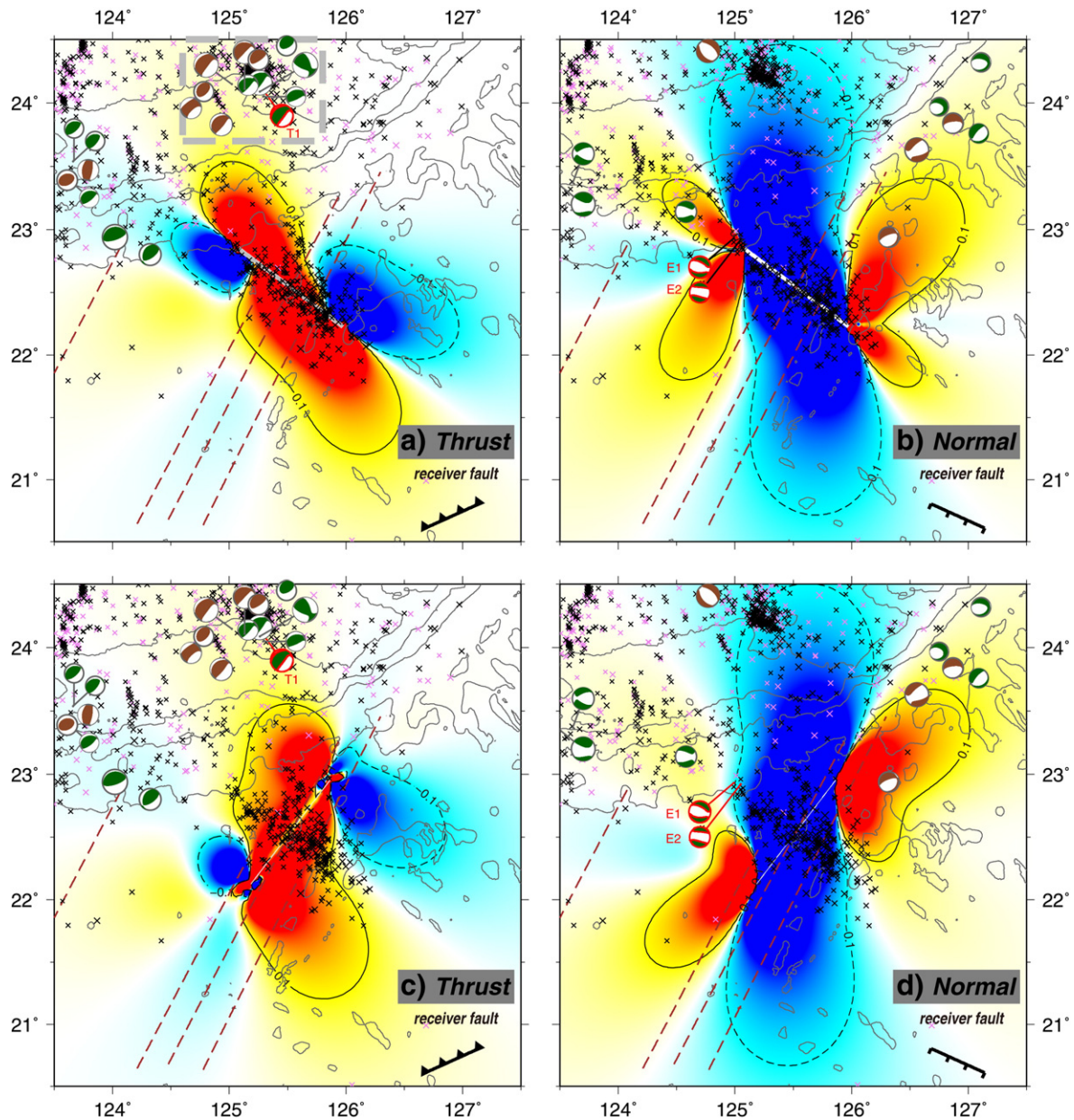


Fig. 5. The ΔCFS calculated based on the two constructed receiver faults T1 (a and c) and E1 (b and d). The source fault is F1' in (a) and (b), whereas it is F2' in (c) and (d). The pink and black crosses show the 3-year pre-shocks and aftershocks with a magnitude $M_w \geq 3$. The brown and green focal mechanisms, extracted from the GCMT catalog for the time period between January 1, 1976 and August 31, 2014, show the pre-shocks and aftershocks of the 1998 mainshock, respectively. Only thrusting type focal mechanisms in (a) and (c) and only normal type in (b) and (d) are plotted.

4.3. The triggering effect for the large intraplate earthquakes in the WPB

To investigate the triggering process of the large intraplate oceanic earthquakes in the WPB, the ΔCFS of the 1998 M_w 7.4 and 2009 M_w 6.9 events was calculated based on a vertical NW–SE fault plane with left-lateral motion. The ΔCFS at the source depth of the 1998 mainshock was extracted to evaluate the influence the effect of the 1998 mainshock to the 2009 event. Although the 2009 event is located at the positive ΔCFS area of the 1998 mainshock, the value of the ΔCFS induced by the 1998 event seems too small to trigger the 2009 earthquake. Thus, we suggest that no clear evidence exists for a triggering effect between the relatively larger intraplate earthquakes in the WPB. However, several earthquakes with no focal mechanism are located in the joint area of the high ΔCFS of the two events. Thus, though the triggering process between the large strike-slip earthquakes and its sequences might not

exist, we suggest that the combination their effect might promote the generation of relatively smaller earthquakes in the positive ΔCFS area.

5. Conclusions

East of Taiwan, the oceanic basin is characterized by several strike-slip events. Based on bathymetry and magnetic anomaly data, obvious NE–SW ancient fracture zones have been identified in the WPB and are considered to be the main rupture plane of these strike-slip earthquakes. However, the aftershock distributions of these strike-slip earthquakes show a NW–SE trending pattern that is almost orthogonal to the fracture zone orientation. In our study, we calculate the ΔCFS induced by the 1998 M_w 7.4 strike-slip earthquake and compared them with the aftershock distribution to determine the rupture plane. Our results show that when both the source and receiver fault planes

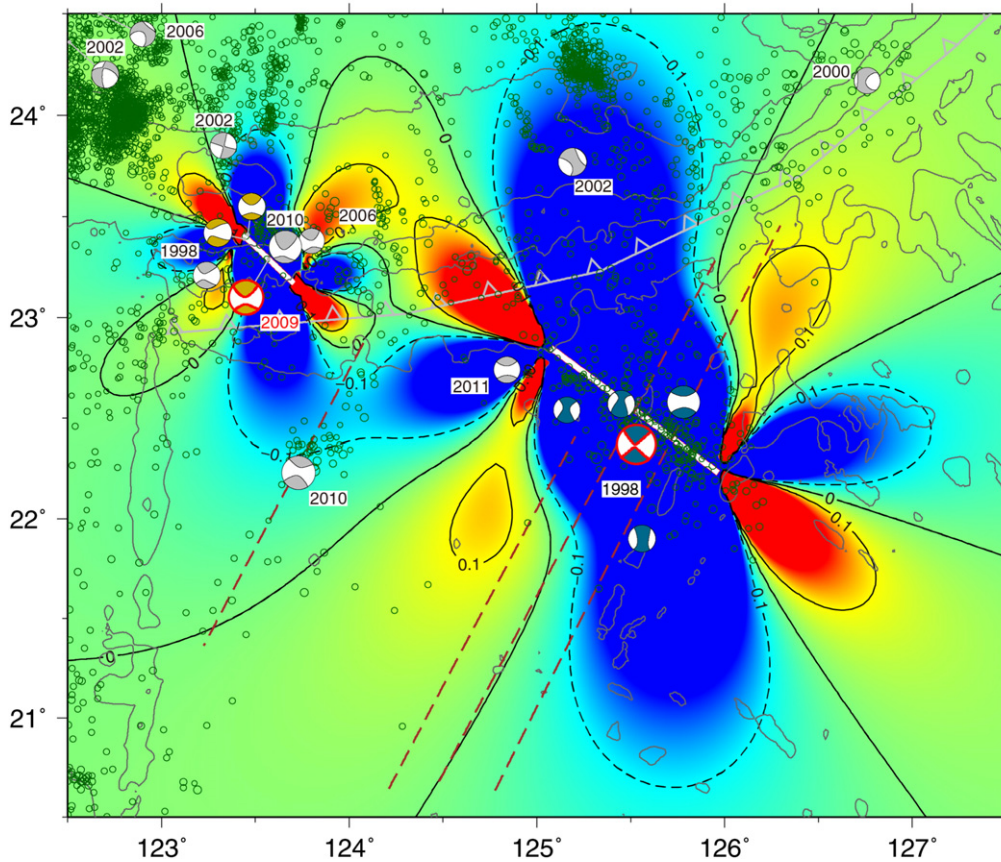


Fig. 6. The ΔCFS distribution induced by the May 3, 1998 M_w 7.4 and August 17, 2009 M_w 6.7 earthquakes at depth of 22.9 km. The calculation is based on a vertical NW–SE fault plane with left-lateral motion. The thick white line shows the surface projection of the rupture plane. The hollow circles are the aftershocks of the 1998 event that occurred between the occurrence of the mainshock and December 30, 2011. The gold and blue color focal mechanisms represent the sequence of the August 17, 2009, M_w 6.7 earthquake and the May 3, 1998, M_w 7.4 earthquake, respectively. The focal mechanisms with the red contour are the position of the two mainshocks. The number marked above the gray focal mechanism represents the year of the occurrence of earthquakes.

are trending in the NW–SE direction, the aftershocks that occurred in the region show good agreement with the maximal ΔCFS . Consequently, we suggest that the 1998 strike-slip events that occurred in the WPB should rupture along the NW–SE direction.

Based on the earthquakes distribution determined from ocean bottom seismometers, Lin et al. (2013a, 2013b) shows that the seismic activity occurred in the oceanic plate instead of following the pre-existing fracture zones and are located along a conjugate fault set with an intersection angle of approximately 120° . Thus, our analyses confirm this suggestion and show that the main rupture plane does strike along the NW–SE direction, which should be the result of the present-day stress regime that exists in the oceanic plate. Moreover, we also observed a concentration of normal faulting and thrusting events in the high ΔCFS area when the receiver fault is of the extensional and compressive type, respectively. The compressive and extensional earthquakes in the area are strongly linked to the subduction process. Thus, we suggest that the occurrence of the strike-slip earthquake in the oceanic intraplate may enhance the seismic activity near the subduction system, particularly for the outer-rise area. This observation may introduce a new concept for the investigation of the seismic hazard for the subduction areas. However, more studies are required to disclose a more detailed and precise relationship between the intra-oceanic plate and subduction-related earthquakes.

Acknowledgments

We thank Editor and two anonymous reviewers for their helpful comments. Many thanks to Dr. W.-L. Chang and Dr. W.-N. Wu for the

pertinent discussions. The GMT software package was used to make all the figures (Wessel and Smith, 1998). Support from the Ministry of Science and Technology, Taiwan, under contract No. 104-2811-M-008-029 and 104-3113-M-008-001 is gratefully acknowledged.

References

- Ando, M., Nakamura, M., Matsumoto, T., Furukawa, M., Tadokoro, K., Furumoto, M., 2009. Is the Ryukyu subduction zone in Japan coupled or decoupled?—The necessity of seafloor crustal deformation observation. *Earth Planets Space* 61, 1031–1039.
- Arnadóttir, T., Jónsson, S., Pedersen, R., Gudmundsson, G.B., 2003. Coulomb stress changes in the South Iceland Seismic Zone due to two large earthquakes in June 2000. *Geophys. Res. Lett.* 30, 1205. <http://dx.doi.org/10.1029/2002GL016495>.
- Chang, C.M., 2007. Seafloor structures in western West Philippine Basin (Master thesis) Institute of Geophysics, National Central University, Taiwan (42 pp., in Chinese).
- Cocco, M., Rice, J.R., 2002. Pore pressure and poroelasticity effects in Coulomb stress analysis of earthquake interactions. *J. Geophys. Res.* 107 ESE 2-1–ESE 2-17.
- Deplus, C., Diament, M., Hébert, H., Bertrand, G., Dominguez, S., Dubois, J., Malod, J., Patriat, P., Pontoise, B., Sibilla, J.-J., 1998. Direct evidence of active deformation in the eastern Indian oceanic plate. *Geology* 26, 131–134.
- Dziewonski, A., Chou, T.A., Woodhouse, J., 1981. Determination of earthquake source parameters from waveform data for studies of global and regional seismicity. *J. Geophys. Res.* 86, 2825–2852.
- Harris, R.A., 1998. Introduction to special section: stress triggers, stress shadows, and implications for seismic hazard. *J. Geophys. Res.* 103, 24347–24358.
- Hsu, S.-K., Yeh, Y.-C., Sibuet, J.-C., Doo, W.-B., Tsai, C.-H., 2013. A mega-splay fault system and tsunami hazard in the southern Ryukyu subduction zone. *Earth Planet. Sci. Lett.* 362, 99–107.
- King, G.C., Stein, R.S., Lin, J., 1994. Static stress changes and the triggering of earthquakes. *Bull. Seismol. Soc. Am.* 84, 935–953.
- Lin, J., Stein, R.S., 2004. Stress triggering in thrust and subduction earthquakes and stress interaction between the southern San Andreas and nearby thrust and strike-slip faults. *J. Geophys. Res.* 109, B02303. <http://dx.doi.org/10.1029/2003JB002607>.
- Lin, J.-Y., Le Pichon, X., Rangin, C., Sibuet, J.C., Maury, T., 2009. Spatial aftershock distribution of the 26 December 2004 great Sumatra–Andaman earthquake in the

- northern Sumatra area. *Geochem. Geophys. Geosyst.* 10, Q05006. <http://dx.doi.org/10.1029/2009GC002454>.
- Lin, J.-Y., Chen, Y.F., Lee, C.S., Hsu, S.K., Liang, C.W., Lin, Y.C., Hsieh, H.S., 2013a. Strike-slip intraplate earthquakes in the Western Philippine Sea Plate. *Tectonophysics* 608, 499–504.
- Lin, J.-Y., Hsu, S.-K., Sibuet, J.-C., Lee, C.-S., Liang, C.-W., 2013b. Plate tearing in the northwestern corner of the subducting Philippine Sea Plate. *J. Asian Earth Sci.* 70, 1–7.
- Lin, J.-Y., Sibuet, J.-C., Hsu, S.-K., Wu, W.-N., 2014. Could a Sumatra-like megathrust earthquake occur in the south Ryukyu subduction zone? *Earth Planets Space* 66, 1–8.
- Ma, K.F., Chan, C.H., Stein, R.S., 2005. Response of seismicity to Coulomb stress triggers and shadows of the 1999 $M_w = 7.6$ Chi-Chi, Taiwan, earthquake. *J. Geophys. Res.* 110, B05S19. <http://dx.doi.org/10.1029/2004JB003389>.
- Meng, L., Ampuero, J.-P., Stock, J., Duputel, Z., Luo, Y., Tsai, V., 2012. Earthquake in a maze: compressional rupture branching during the 2012 M_w 8.6 Sumatra earthquake. *Science* 337, 724–726.
- Nakamura, M., 2006. Source fault model of the 1771 Yaeyama tsunami, southern Ryukyu Islands, Japan, inferred from numerical simulation. *Pure Appl. Geophys.* 163, 41–54.
- Nakamura, M., 2009. Fault model of the 1771 Yaeyama earthquake along the Ryukyu Trench estimated from the devastating tsunami. *Geophys. Res. Lett.* 36, L19307. <http://dx.doi.org/10.1029/2009GL039730>.
- Nostro, C., Chiaraluce, L., Cocco, M., Baumont, D., Scotti, O., 2005. Coulomb stress changes caused by repeated normal faulting earthquakes during the 1997 Umbria–Marche (central Italy) seismic sequence. *J. Geophys. Res.* 110, B05S20. <http://dx.doi.org/10.1029/2004JB003386>.
- Okada, Y., 1985. Surface deformation due to shear and tensile faults in a half-space. *Bull. Seismol. Soc. Am.* 75, 1135–1154.
- Parsons, T., Stein, R.S., Simpson, R.W., Reasenber, P.A., 1999. Stress sensitivity of fault seismicity: a comparison between limited-offset oblique and major strike-slip faults. *J. Geophys. Res.* 104, 20183–20202.
- Skempton, A., 1954. The pore-pressure coefficients A and B. *Geotechnique* 4, 143–147.
- Stein, R.S., King, G.C., Lin, J., 1992. Change in failure stress on the southern San Andreas fault system caused by the 1992 magnitude = 7.4 Landers earthquake. *Science* 258, 1328–1332.
- Wang, W.-H., Chen, C.-H., 2001. Static stress transferred by the 1999 Chi-Chi, Taiwan, earthquake: Effects on the stability of the surrounding fault systems and aftershock triggering with a 3D fault-slip model. *Bull. Seismol. Soc. Am.* 91, 1041–1052.
- Wells, D.L., Coppersmith, K.J., 1994. New empirical relationships among magnitude, rupture length, rupture width, rupture area, and surface displacement. *Bull. Seismol. Soc. Am.* 84, 974–1002.
- Wessel, P., Smith, W.H.F., 1998. New improved version of generic mapping tools. *EOS Trans. Am. Geophys. Union* 79, 579.
- Wiemer, S., Wyss, M., 2000. Minimum magnitude of completeness in earthquake catalogs: examples from Alaska, the western United States, and Japan. *Bull. Seismol. Soc. Am.* 90, 859–869.
- Wu, W.N., Kao, H., Hsu, S.K., Lo, C.L., Chen, H.W., 2010. Spatial variation of the crustal stress field along the Ryukyu–Taiwan–Luzon convergent boundary. *J. Geophys. Res.* 115, B11401. <http://dx.doi.org/10.1029/2009JB007080>.
- Yu, S.-B., Chen, H.-Y., Kuo, L.-C., 1997. Velocity field of GPS stations in the Taiwan area. *Tectonophysics* 274, 41–59.
- Yue, H., Lay, T., Koper, K.D., 2012. En echelon and orthogonal fault ruptures of the 11 April 2012 great intraplate earthquakes. *Nature* 490, 245–249.